Supporting Information for

Intriguing Near-Infrared Solid-State Luminescence of Binuclear Silver(I) Complexes Based on Pyridylphospholane Scaffolds

Aliia V. Shamsieva,*† Elvira I. Musina, † Tatiana P. Gerasimova, † Robert R. Fayzullin, † Ilya E. Kolesnikov,‡ Aida I. Samigullina, † Sergey A. Katsyuba, † Andrey A. Karasik, † Oleg G. Sinyashin†

† Arbuzov Institute of Organic and Physical Chemistry, FRC Kazan Scientific Center, Russian Academy of Sciences, Arbuzov Street 8, 420088 Kazan, Russian Federation
‡ Center for Optical and Laser Materials research, Research Park of St. Petersburg State University, Ulianovskaya Street 5, 198504 St. Petersburg, Russia

shamsieva.aliya@mail.ru

Table of contents

General information.

All reactions and manipulations were carried out under a dry argon atmosphere by using standard vacuum-line techniques. Commercially available solvents were purified, dried, deoxygenated, and distilled before use.

^{1}H NMR (400 MHz) and ^{31}P NMR (162 MHz) spectra were recorded on a Bruker Avance-DRX 400 spectrometer by using the residual solvent as an internal reference for ^{1}H (δ = 1.94 ppm in CD_3CN) and 85% aqueous solution of H_3PO_4 as an external reference for ^{31}P. Chemical shifts are reported in ppm and coupling constants (*J*) are reported in Hz.

ESI measurements were performed using an AmaZon X ion trap mass spectrometer in positive and negative modes. The mass spectral data were processed using the program XCalibur. The mass spectra are given as *m/z* values and relative intensities (I_{rel}, %). Acetonitrile was used as solvent for mass-spectrometry measurements.

IR spectra in the 4000-400 cm^{-1} regions were recorded on a Bruker FTIR spectrometer Tensor 27 with an optical resolution of 4 cm^{-1} and accumulation of 32 scans. To register the IR spectra of complexes **4** – **6**, the samples were compressed into tablets with the addition of KBr.

IR spectra in the range of 100–600 cm^{-1} were recorded on a Bruker FTIR spectrometer IFS 66v at a resolution of 1 cm^{-1}. Solid samples were prepared as polyethylene pellets.

Elemental analysis was carried out on “EuroVector-3000”. Detection of phosphorus was provided by combustion in an oxygen stream.

Photophysical measurements. UV/VIS spectra were registered at room temperature on a Perkin-Elmer Lambda 35 spectrometer with a scan speed of 480 nm min^{-1}, using a spectral width of 1 nm. The excitation and emission spectra for the solid-state samples at room temperature were measured on Fluorolog-3 (Horiba Jobin Yvon) spectrofluorimeter. The powder samples were supported on the quartz glass plates. LEDs (maximum of emission at 265 nm, 340 nm and 390 nm) were used in pulse mode to pump the luminescence in lifetime measurements (pulse width 1 ns, repetition rate 100 kHz). The interference filters (399, 450 nm) were used to cut-off high diffraction orders. The integration sphere (Quanta–φ, 6 inches) was used to measure the solid-state emission quantum yield for the complexes **4** – **6**. The measurements were carried out with powders according to the guide provided by manufacturer (four spectra-based measurement). Three samples of each complex were measured to increase the accuracy. The emission and excitation spectra of solutions were recorded at room temperature on a Varian Cary Eclipse Fluorescence Spectrophotometer, using 10 mm quartz cells. All samples were prepared as solutions in acetonitrile with a concentration of $2.7 \cdot 10^{-4}$ $mol \cdot L^{-1}$. The absorbance at excitation wavelength was less than 0.1 to avoid the ‘‘inner filter effect’’.

Computational Methods. Quantum chemical calculations were performed with the Gaussian-16[1] suite of programs. The hybrid PBE0 functional[2] and the Ahlrichs’ triple-ζ def-TZVP AO basis set[3] were used for optimization of triplet structure of dicationic part of complex **4. T**he D3 approach[4] to describe the London dispersion interactions together with the Becke–Johnson (BJ) damping function[5–7] were employed as implemented in the Gaussian-16 program. Time-Dependent Density Functional Response Theory (TD-DFT) has been employed to compute the vertical excitation energies (i.e., absorption wavelengths) and oscillator strengths on the X-ray geometries in the gas phase. 50 lowest singlet excited states were taken into account. The procedure was analogous to the one described elsewhere[8]. For TD-DFT computations B3LYP[9,10] functional was used in combination with 6-31G* basis sets on C, H, N, B, F and P atoms [11,12] and SBKJC effective-core potentials with VDZ valence double-ζ electrons for Ag.[13–15] The percentage contributions of atoms/atom group to the molecular orbitals were calculated with GaussSum program.[16]

X-ray diffraction studies. X-ray diffraction (XRD) data for the single crystals of **4**, **5**, and **6** were collected on a Bruker Kappa Apex II CCD diffractometer using graphite monochromated Mo*Kα* (0.71073 Å) radiation at 150(2), 173(2), and 100(2) K, respectively. The performance mode of the sealed X-ray tube was 50 kV, 30 mA. The diffractometer was equipped with an Oxford Cryostream LT device. Suitable crystals of appropriate dimensions were mounted on glass fibres or cactus needles in random orientations. Preliminary unit cell parameters were determined with three sets of a total of 12 narrow frame scans. The data were collected according to recommended strategies in an ω/φ-scan mode. Data collection: images were indexed and integrated using the APEX3 data reduction package (v2015.9-0, Bruker AXS). Final cell constants were determined by global refinement of reflections from the complete

data set. Analysis of the integrated data did not show any decay. Data were corrected for systematic errors and absorption by means of SADABS-2014/5 based on the Laue symmetry using equivalent reflections. Analysis of the integrated data did not show any decay. XPREP-2014/2 and the ASSIGN SPACEGROUP routine of WinGX were used for analysis of systematic absences and space group determination. The structures were solved by the direct methods using SHELXT-2018/2 [17] and refined by the full-matrix least-squares on F^2 using SHELXL-2018/3.[18] Calculations were mainly performed using the WinGX-2018.3 suite of programs.[19] Non-hydrogen atoms were refined anisotropically. The positions of the hydrogen atoms of methyl groups were found using rotating group refinement with idealized tetrahedral angles. The other hydrogen atoms were inserted at the calculated positions and refined as riding atoms. Disorder of tetrafluoroborate anions, if present, was resolved using free variables and reasonable restraints on geometry and anisotropic displacement parameters. Interestingly, all the complexes crystallize with molecules divided into exactly equal parts according to crystallographic symmetry (an inversion center), hence the asymmetric cells contain half (Z' = 0.5) of the cationic complexes. All the compounds studied have no unusual bond lengths and angles.
Calculation of the Kitaigorodsky parking indexes was performed using the PLATON-200618 crystallographic tool.[20]

Crystallographic data for 4. $C_{18}H_{24}Ag_2B_2F_8N_2P_2$, colorless prism (0.460 × 0.372 × 0.190 mm^3), formula weight 719.69, monoclinic, $P2_1/c$ (No. 14), a = 7.275(2) Å, b = 16.022(5) Å, c = 10.252(3) Å, β = 92.067(4)°, V = 1194.2(6) Å^3, Z = 2, Z' = 0.5, T = 150(2) K, d_{calc} = 2.001 g cm^{-3}, μ(MoK_α) = 1.847 mm^{-1}, F(000) = 704; $T_{max/min}$ = 0.7460/0.5481; 13557 reflections were collected (2.360° ≤ θ ≤ 27.248°), 2677 of which were unique, R_{int} = 0.0618, R_σ = 0.0459; completeness to θ of 25.242° 100 %. The refinement of 191 parameters with 94 restraints converged to R_1 = 0.0389 and wR_2 = 0.1010 for 2259 reflections with $I > 2\sigma(I)$ and R_1 = 0.0477 and wR_2 = 0.1069 for all data with S = 1.026 and residual electron density, $\rho_{max/min}$ = 1.300 and –0.925 e Å^{-3}.
Crystallographic data for 5. $C_{20}H_{28}Ag_2B_2F_8N_2P_2$, colorless plate (0.361 × 0.211 × 0.090 mm^3), formula weight 747.74, monoclinic, $P2_1/c$ (No. 14), a = 8.1488(9) Å, b = 17.998(2) Å, c = 8.8905(10) Å, β = 101.714(5)°, V = 1276.8(3) Å^3, Z = 2, Z' = 0.5, T = 173(2) K, d_{calc} = 1.945 g cm^{-3}, μ(MoK_α) = 1.731 mm^{-1}, F(000) = 736; $T_{max/min}$ = 0.7358/0.5655; 17221 reflections were collected (3.964° ≤ θ ≤ 26.750°), 2690 of which were unique, R_{int} = 0.0520, R_σ = 0.0421; completeness to θ of 25.242° 98.8 %. The refinement of 210 parameters with 184 restraints converged to R_1 = 0.0382 and wR_2 = 0.0906 for 2072 reflections with $I > 2\sigma(I)$ and R_1 = 0.0554 and wR_2 = 0.1011 for all data with S = 1.052 and residual electron density, $\rho_{max/min}$ = 1.618 and –0.794 e Å^{-3}.
Crystallographic data for 6. $C_{20}H_{28}Ag_2B_2F_8N_2P_2$, colorless plate (0.382 × 0.330 × 0.046 mm^3), formula weight 747.74, monoclinic, $P2_1/n$ (No. 14), a = 6.9245(12) Å, b = 9.9717(14) Å, c = 18.628(4) Å, β = 97.059(12)°, V = 1276.5(4)Å^3, Z = 2, Z' = 0.5, T = 100(2) K, d_{calc} = 1.945 g cm^{-3}, μ(MoK_α) = 1.732 mm^{-1}, F(000) = 736; $T_{max/min}$ = 0.7307/0.6137; 9644 reflections were collected (3.005° ≤ θ ≤ 25.300°), 2246 of which were unique, R_{int} = 0.0799, R_σ = 0.0906; completeness to θ of 25.242° 96.3 %. The refinement of 164 parameters with no restraints converged to R_1 = 0.0465 and wR_2 = 0.0816 for 1512 reflections with $I > 2\sigma(I)$ and R_1 = 0.0925 and wR_2 = 0.0935 for all data with S = 1.029 and residual electron density, $\rho_{max/min}$ = 0.977 and –0.768 e Å^{-3}.
The crystallographic data for the investigated compounds have been deposited in the Cambridge Crystallographic Data Centre as supplementary publication numbers CCDC 1862201 (**4**), 1862202 (**5**), and 1862203 (**6**). These data can be obtained free of charge via www.ccdc.cam.ac.uk/data_request/cif, or by emailing data_request@ccdc.cam.ac.uk, or by contacting The Cambridge Crystallographic Data Centre, 12 Union Road, Cambridge CB2 1EZ, UK; fax: +44 1223 336033.

The powder X-ray diffraction studies were performed on an automated Bruker D8 Advance X-ray diffractometer equipped with a Vario setup and a Vantec linear coordinate detector. The Cu$K\alpha_1$ radiation monochromated by a curved Johansson monochromator (1.5406 Å) was used, and the performance mode of the sealed X-ray tube was 40 kV, 40 mA. All experiments were carried out at room temperature (293(2) K) in the Bragg–Brentano geometry. Powder samples were placed in a zero-diffraction holder. Patterns were recorded in the 2θ range between 5 and 42°, in 0.016°steps, with a step time of 0.2 s and rotation 15 rpm.

Synthetic procedure.

The ligands **1** – **3** were synthesized and characterized according to the described methodology. [21]

Synthesis of bis-(μ-[2-(phospholan-1-yl)pyridine]-P,N) disilver(I) bis(tetrafluoroborate) 4.

To a solution of **1** (1.8 mmol) in CH_2Cl_2 (3 ml) suspension of silver(I) tetrafluoroborate (1.8 mmol) in CH_2Cl_2 (10 ml) was added. The colour of reaction mixture changed from pale-yellow to reddish-brown and accompanied by precipitation of complex **4**. After stirring for 12 h the light-brown precipitate was collected, washed with CH_2Cl_2 and dried under vacuo. Yield: 0.38 g (81%). M.p. = 237° C. ^{1}H NMR (400 MHz, [D$_3$]CH_3CN, 25^{o}C): δ=8.79(ddd, J(H,H) = 5.12 Hz, J(H,H) = 2.3 Hz, J(H,H) = 0.8 Hz, 1H; Py-6), 8.02 (dddd, J(H,H) = 7.8 Hz, J(H,H)=7.7 Hz, J(H,H) = 2.3 Hz, J(P,H)= 1.8 Hz, 1H; Py-4), 7.83 (dddd J(H,H) = 7.8 Hz, J(H,H)= 2.6 Hz, J(H,H)= 0.8 Hz, J(P,H)= 0.8 Hz, 1 H; Py-5), 7.60 (dddd, J(H,H)= 7.7 Hz, J(H,H) = 5.12 Hz, J(H,H) = 2.6 Hz, J(P,H)= 1.2 Hz, 1H; Py-3), 2.43-2.24(m., 4H, P-CH_2-), 2.00-1.92 (m, 4H, C-$(CH_2)_2$-C, partially overlapped with signal of solvent). ^{31}P{^{1}H} NMR (162 MHz, 25^{o}C): δ= 10.0 ppm (s). IR (KBr pellet): 1587 (m), 1575 (w), 1468(w), 1451 (m), 1422 (m), 1068 (vs), 846 (w), 766 (m), 681 (w), 521 (m), 353 (w) cm^{-1}. MS (70 eV): *m/z*(%): 437 (100) [M – Ag – 2BF_4]$^+$. Elemental analysis, calcd.(%) for $C_{19}H_{27}P_2N_2Ag_2B_2F_8$: C 31.06; H 3.70; Ag 29.36; B 2.94; F 20.69; N 3.81; P 8.43; found C 30.04; H 3.3; Ag 29.98; B 3.0; N 3.81; P 8.61. The single crystals of compound **4** used for an XRD study were obtained by slow vapour diffusion of diethyl ether into dichloromethane solution.

General procedure for synthesis of 5 and 6.

To a solution of ligand (**2**, **3**) (1.5 mmol (**2**), 2.5 mmol (**3**)) in CH_3CN (4 ml) a solution of silver(I) tetrafluoroborate (1.5 mmol (for **2**), 2.5 mmol (for **3**)) in CH_3CN (5 ml) was added. Reddish-brown coloured reaction mixture was stirred for 12 h, afterwards the solvent was removed. Pale-brown solids were obtained by washing the residue with ethanol and drying under vacuo.

Bis-(μ-[4-methyl-2-(phospholan-1-yl)pyridine]-P,N) disilver (I) bis(tetrafluoroborate) 5. Yield: 0.41 g (73%). M.p. = 284°C. ^{1}H NMR (400 MHz, [D$_3$]CH_3CN, 25^{o}C): δ=8.62 (d, J(H,H)= 5.28 Hz, 1H, Py-6), 7.65 (w.s., 1H, Py-3), 7.41 (m, 1H, Py-5), 2.47 (s, 3H, -CH_3), 2.22-2.43 (m, 4H, P-CH_2-), 1.97-2.02 (m, 4H, C-$(CH_2)_2$-C, partially overlapped with signal of solvent). ^{31}P{^{1}H} NMR (162 MHz, 25^{o}C): δ= 8.8 ppm (s). IR (KBr pellet): 1601 (s), 1552 (w), 1479 (m), 1449 (w), 1415 (m), 1304 (w), 1287 (w), 1259 (w), 1055 (vs), 848 (s), 836 (s), 766 (w), 688 (w), 546 (w), 521 (m), 503 (w), 441 (m), 352 (w) cm^{-1}. MS (70 eV): *m/z*(%): 465 (100) [M – Ag – 2BF_4]$^+$. Elemental analysis, calcd. (%) for: $C_{21}H_{31}P_2N_2Ag_2B_2F_8$: C 33.07; H 4.10; Ag 28.28; B 2.83; F 19.93; N 3.67; P 8.12; found C 32.81; H 2.29; Ag 29.7; B 2.98; N 3.64; P 8.53. The single crystals of compound **5** used for an XRD study were obtained by slow vapour diffusion of ethanol into dichloromethane solution.

Bis-(μ-[2-methyl-6-(phospholan-1-yl)pyridine]-P,N) disilver (I) bis(tetrafluoroborate) 6. Yield: 0.67 g (70%) M.p. = 273°C. ^{1}H NMR (400 MHz, [D$_3$]CH_3CN, 25^{o}C): δ=7.81 (ddd, J(H,H) = 7.69 Hz, J(H,H) = 7.77 Hz, J(H,H) = 2.74 Hz, 1H, Py-4), 7.57 (dd, J(H,H) = 7.65 Hz, J(H,H) = 7.90 Hz, 1H, Py-5), 7.37 (dd, J(H,H) = 7.34 Hz, J(H,H) = 7.59 Hz, 1H, Py-3), 2.64 (s, 3H, -CH_3), 2.36-2.45 (m, 2H, P-CH_2), 2.19-2.27 (m, 2H, P-CH_2), 1.89-1.96 (m, 4H, C-$(CH_2)_2$-C, partially overlapped with signal of solvent). ^{31}P{^{1}H} NMR (162 MHz, 25^{o}C): δ= 5.3 ppm (s). IR (KBr pellet): 1590 (m), 1561 (w), 1459 (s), 1426 (w), 1377 (w), 1285 (vw), 1258 (vw), 1193 (w), 1053 (vs), 1016 (s), 868 (vw), 841 (w), 800 (m), 764 (vw), 667 (vw), 570 (vw), 520 (m), 506 (w), 424 (w), 352 (w) cm^{-1}. MS (70 eV): *m/z*(%): 465 (100) [M – Ag – 2BF_4]$^+$. Elemental analysis, calcd. (%) for: $C_{21}H_{31}P_2N_2Ag_2B_2F_8$: C 33.07; H 4.10; Ag 28.28; B 2.83; F 19.93; N 3.67; P 8.12; found: C 32.05; H 4.23; Ag 27.8; B 2.9; N 4.0; P 8.54. The single crystals of compound **5** used for an XRD study were obtained by slow vapour diffusion of ethanol into acetonitrile solution.

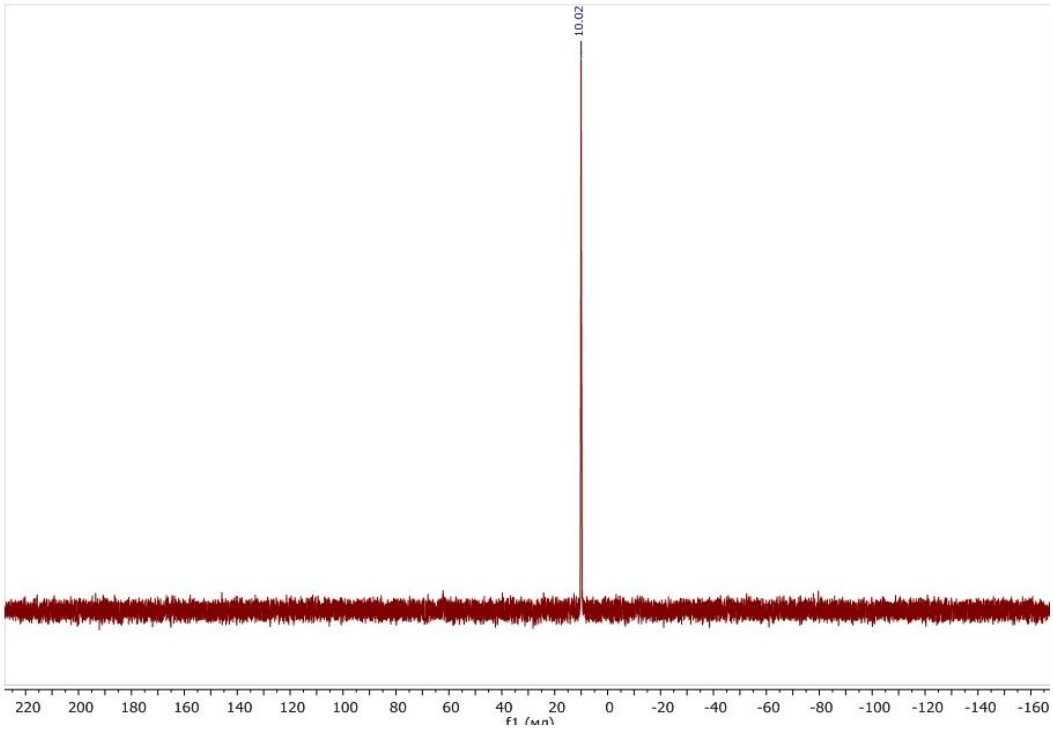

Figure S1. The $^{31}P\{^{1}H\}$ NMR (in CD_3CN) spectrum of complex **4**

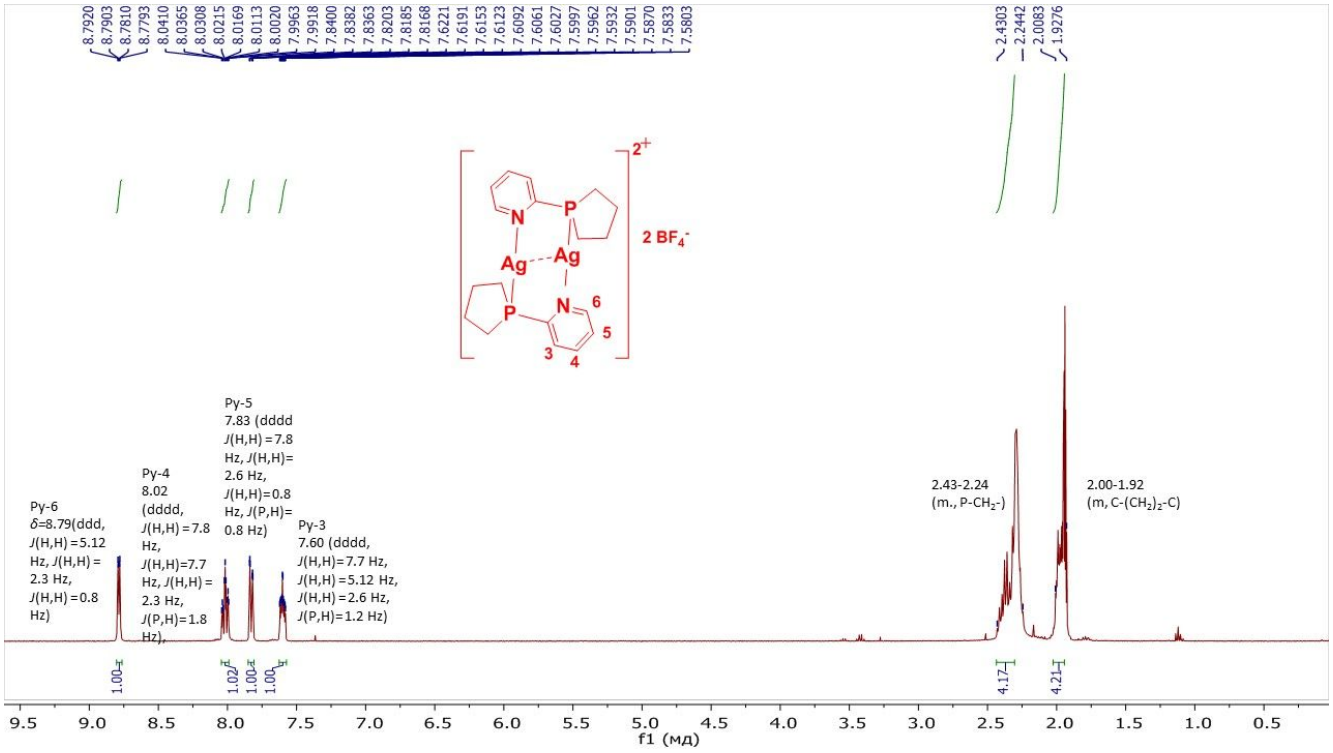

Figure S2. The ^{1}H NMR (in CD_3CN) spectrum of complex **4**

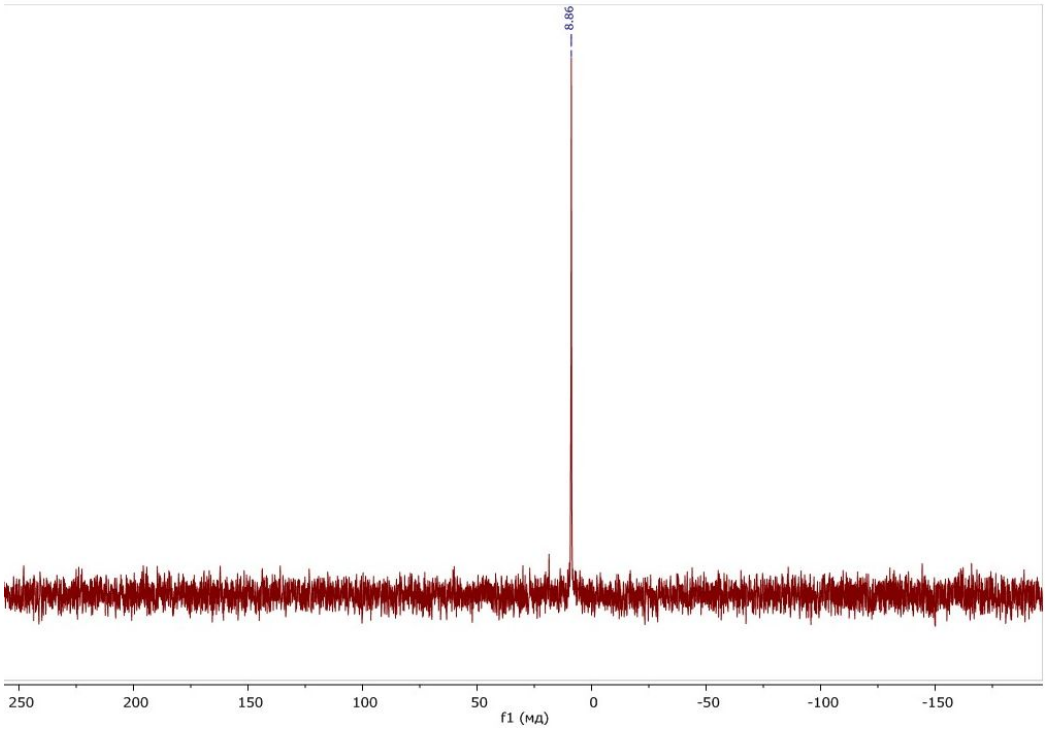

Figure S3. The $^{31}P\{^{1}H\}$ NMR (in CD_3CN) spectrum of complex **5**

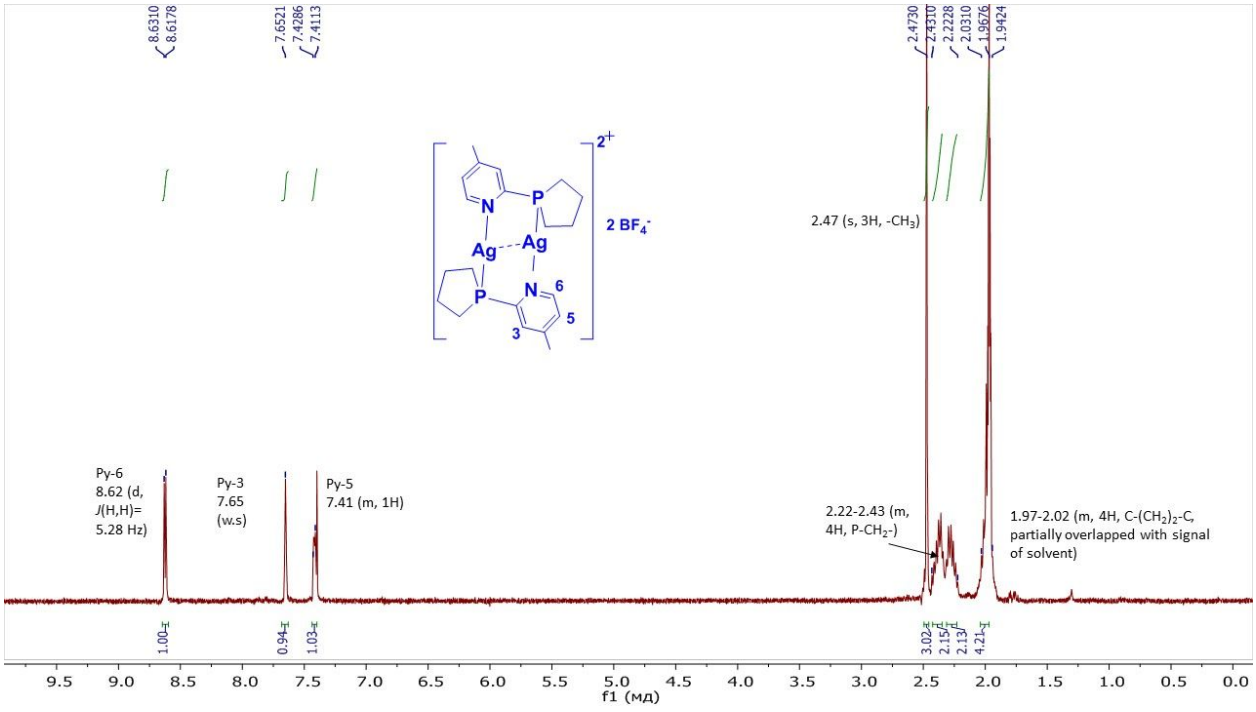

Figure S4. The ^{1}H NMR (in CD_3CN) spectrum of complex **5**

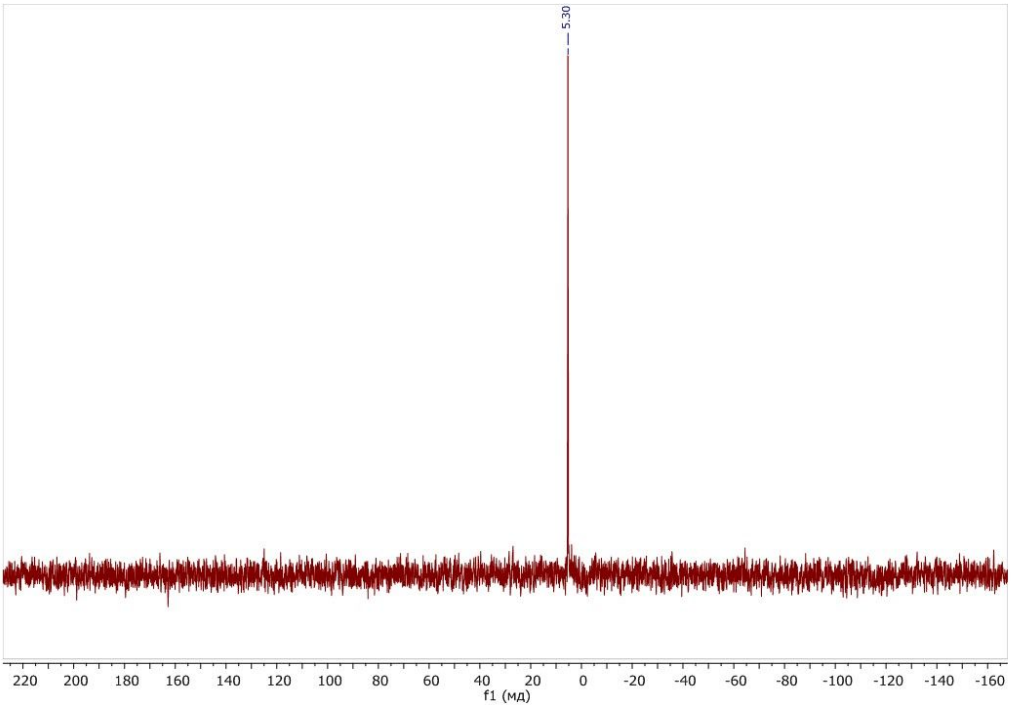

Figure S5. The $^{31}P\{^{1}H\}$ NMR (in CD_3CN) spectrum of complex **6**

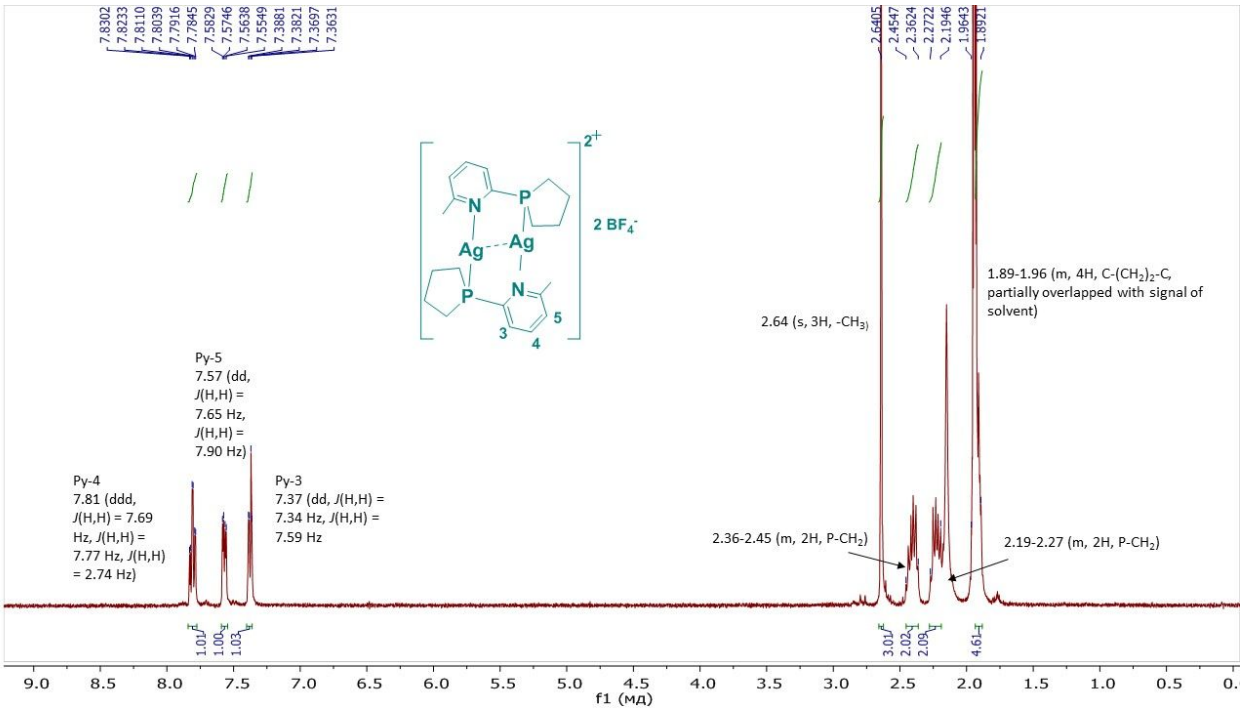

Figure S6. The ^{1}H NMR (in CD_3CN) spectrum of complex **6**

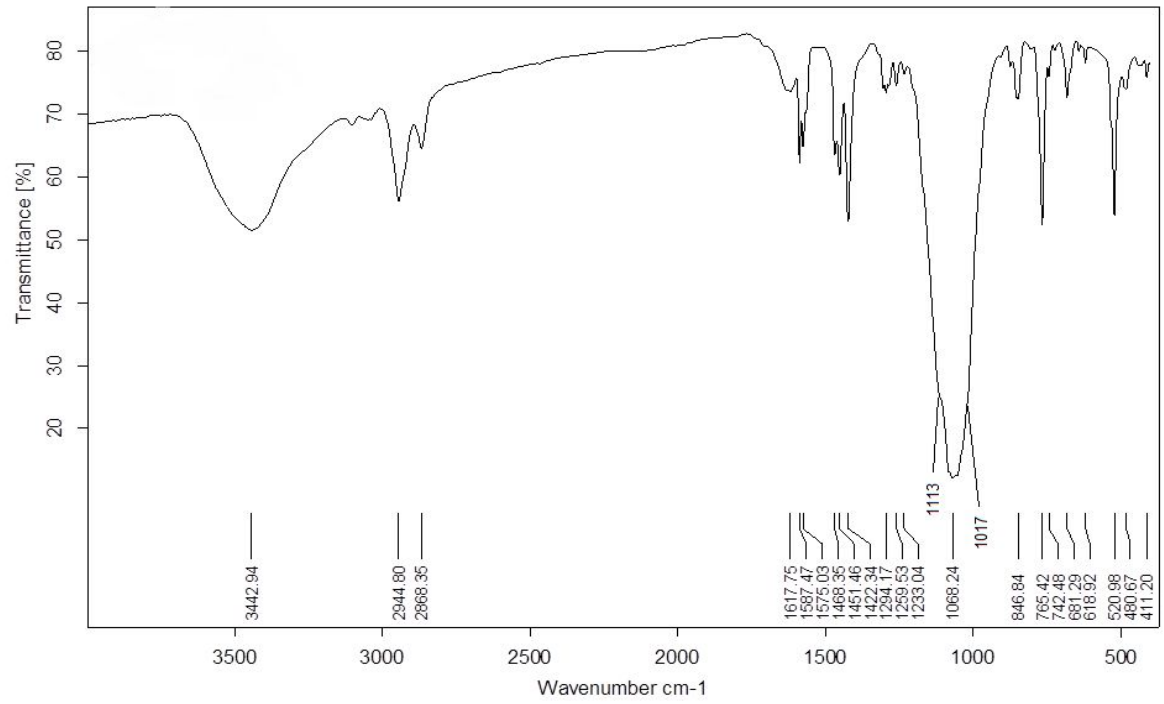

Figure S7. The IR-spectrum of complex **4**

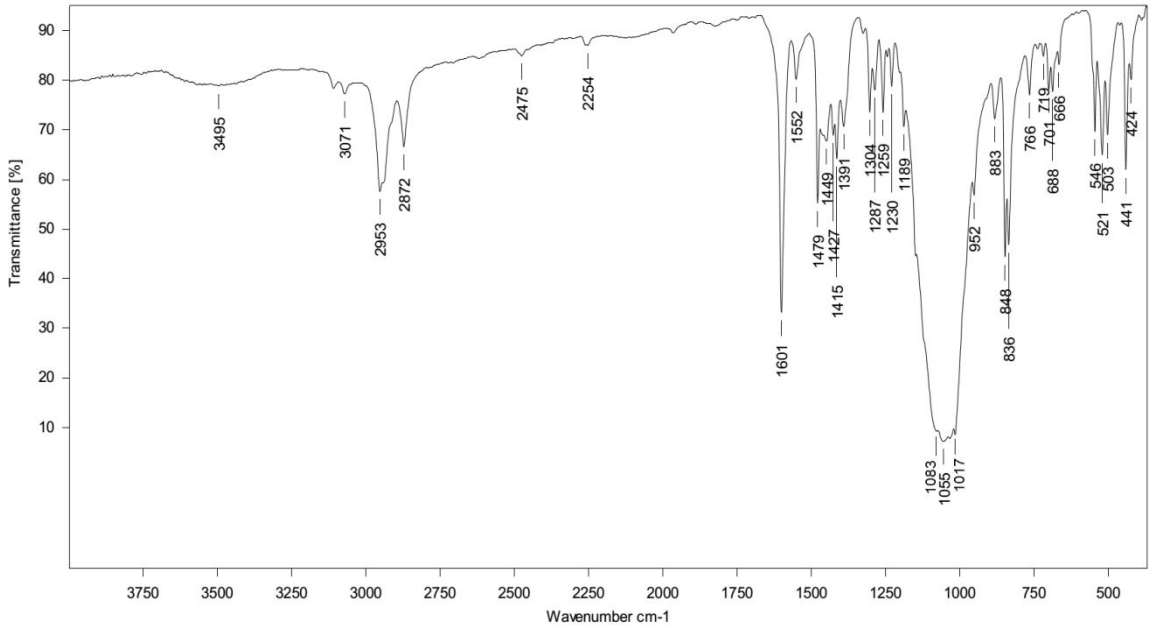

Figure S8. The IR-spectrum of complex **5**

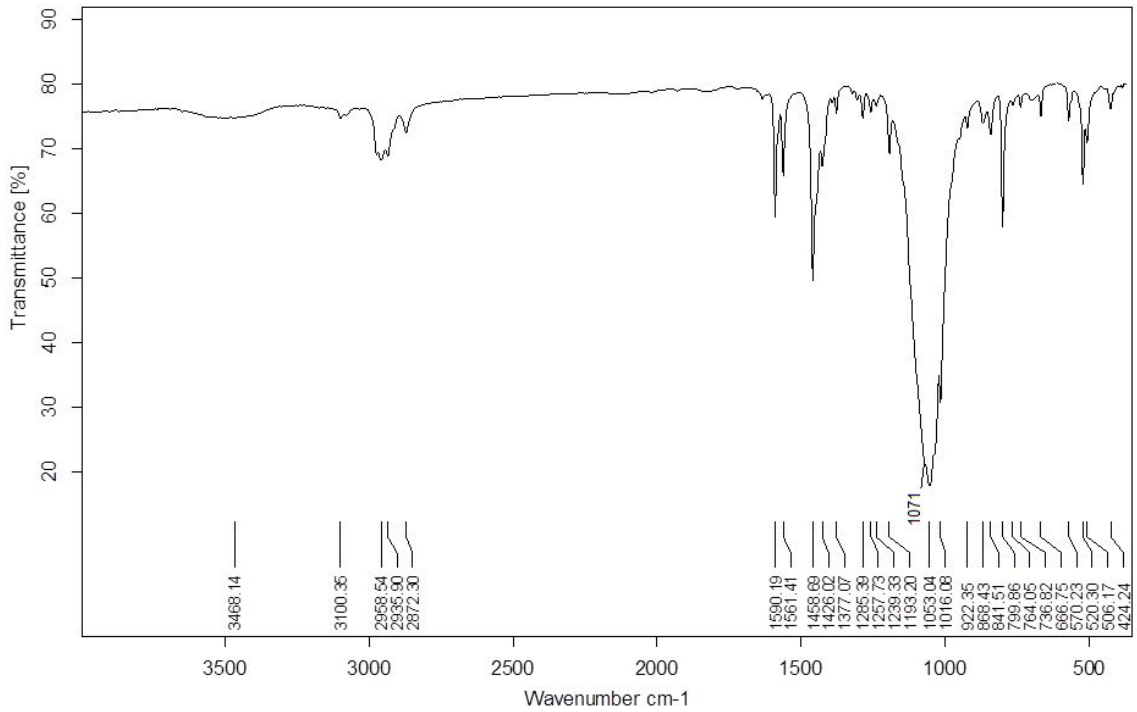

Figure S9. The IR-spectrum of complex **6**

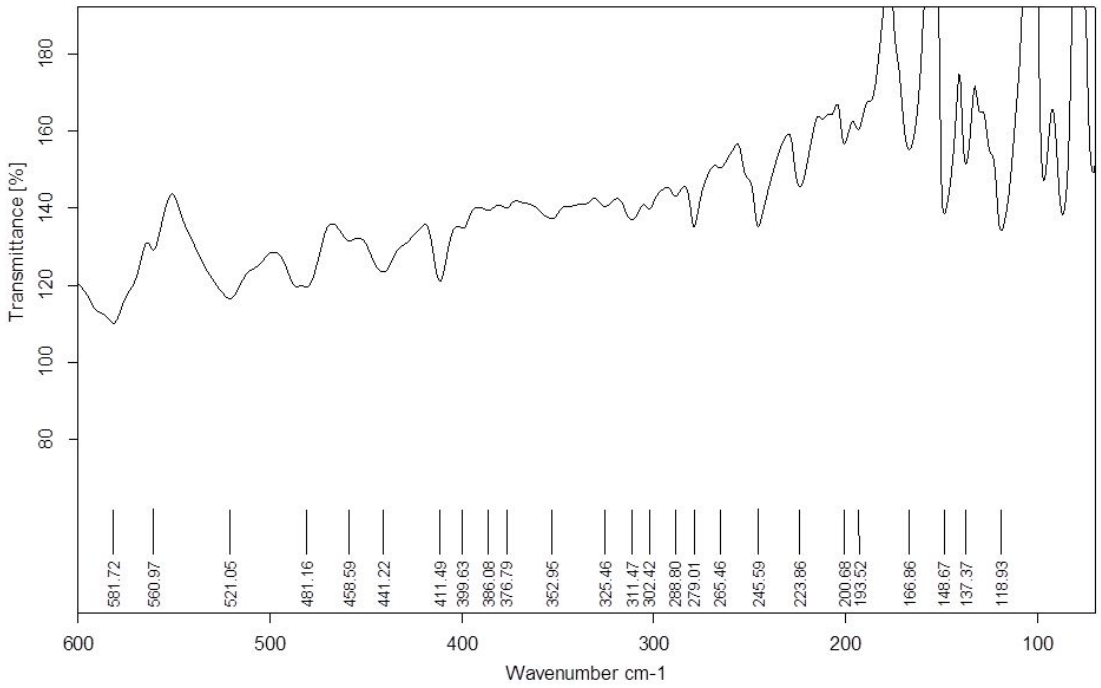

Figure S10. The far IR-spectrum of complex **4**.

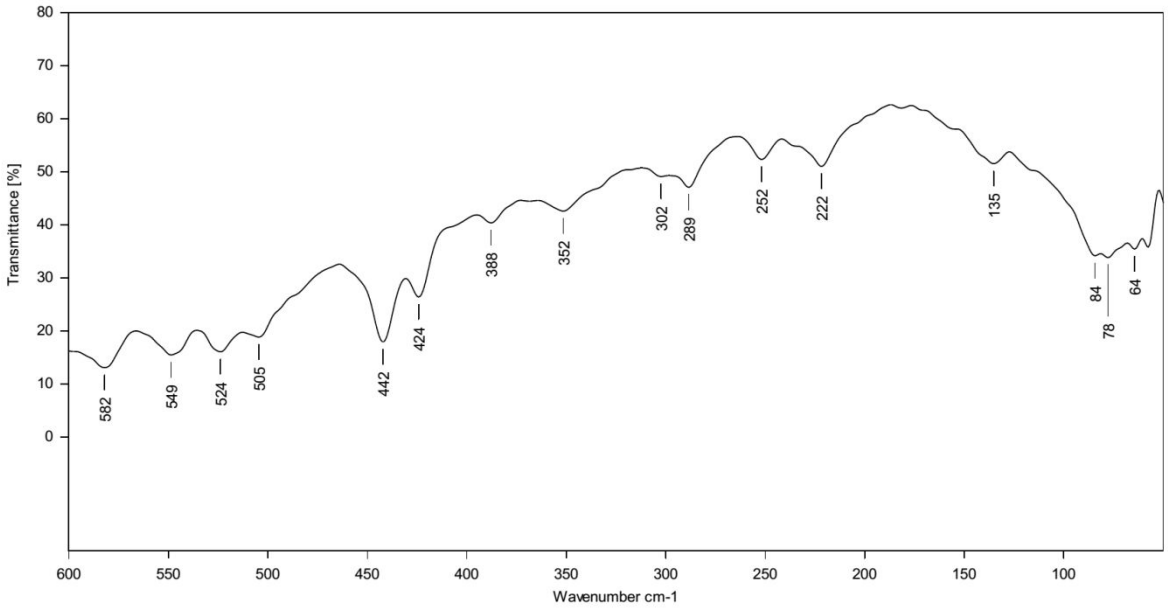

Figure S11. The far IR-spectrum of complex **5**.

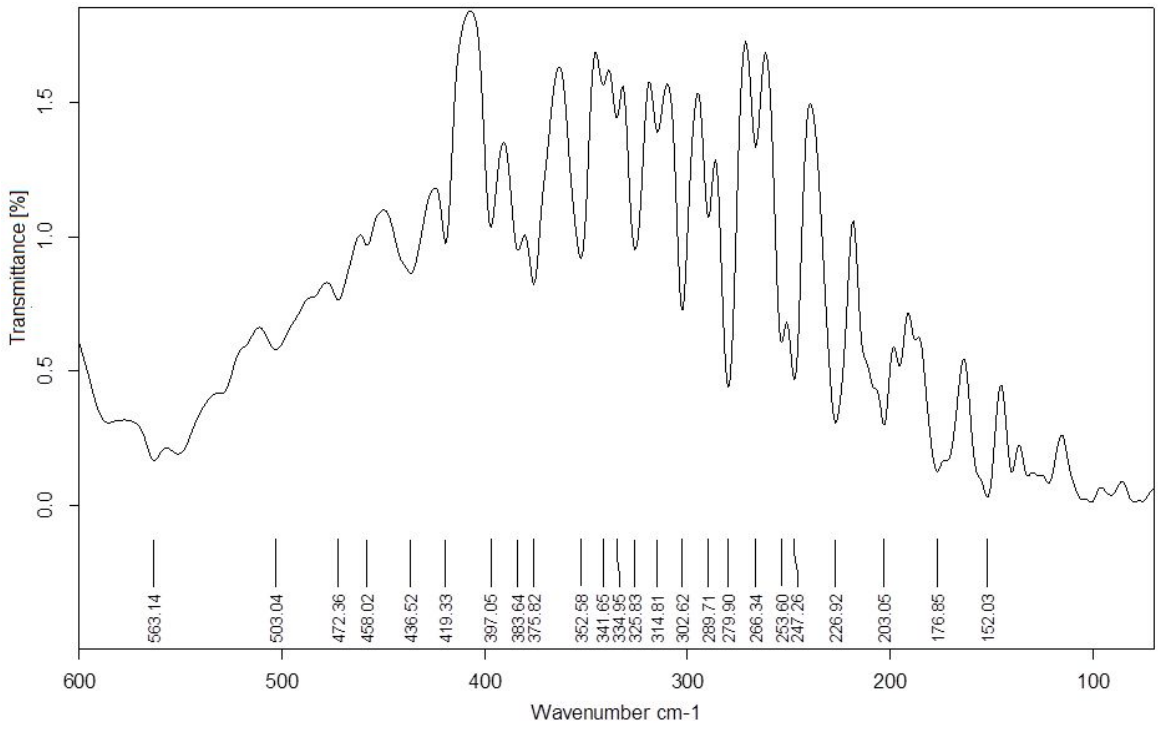

Figure S12. The far IR-spectrum of complex **6**.

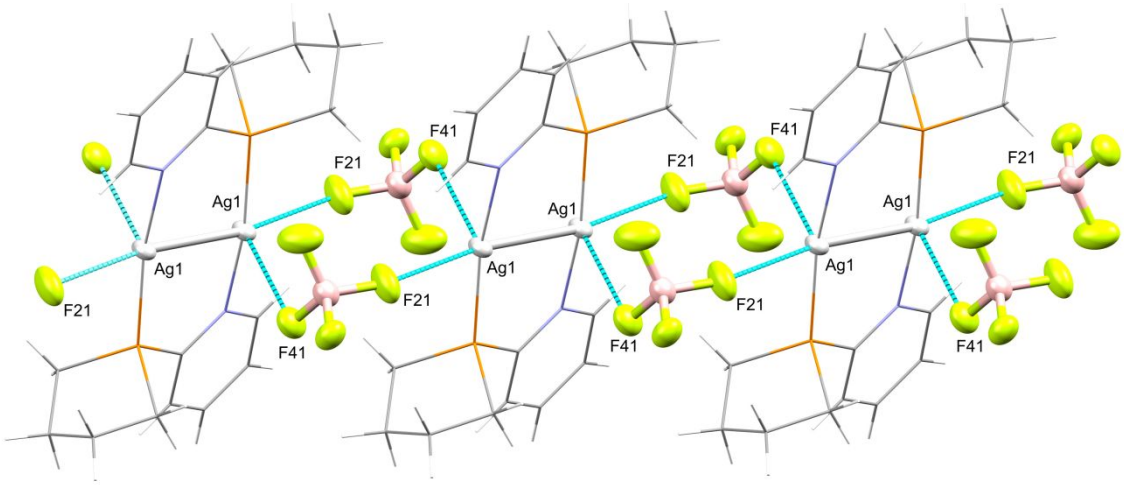

Figure S13. Fragment of crystal packing of complex **4**. Only the main component of disordered tetrafluoroborate anions is shown.

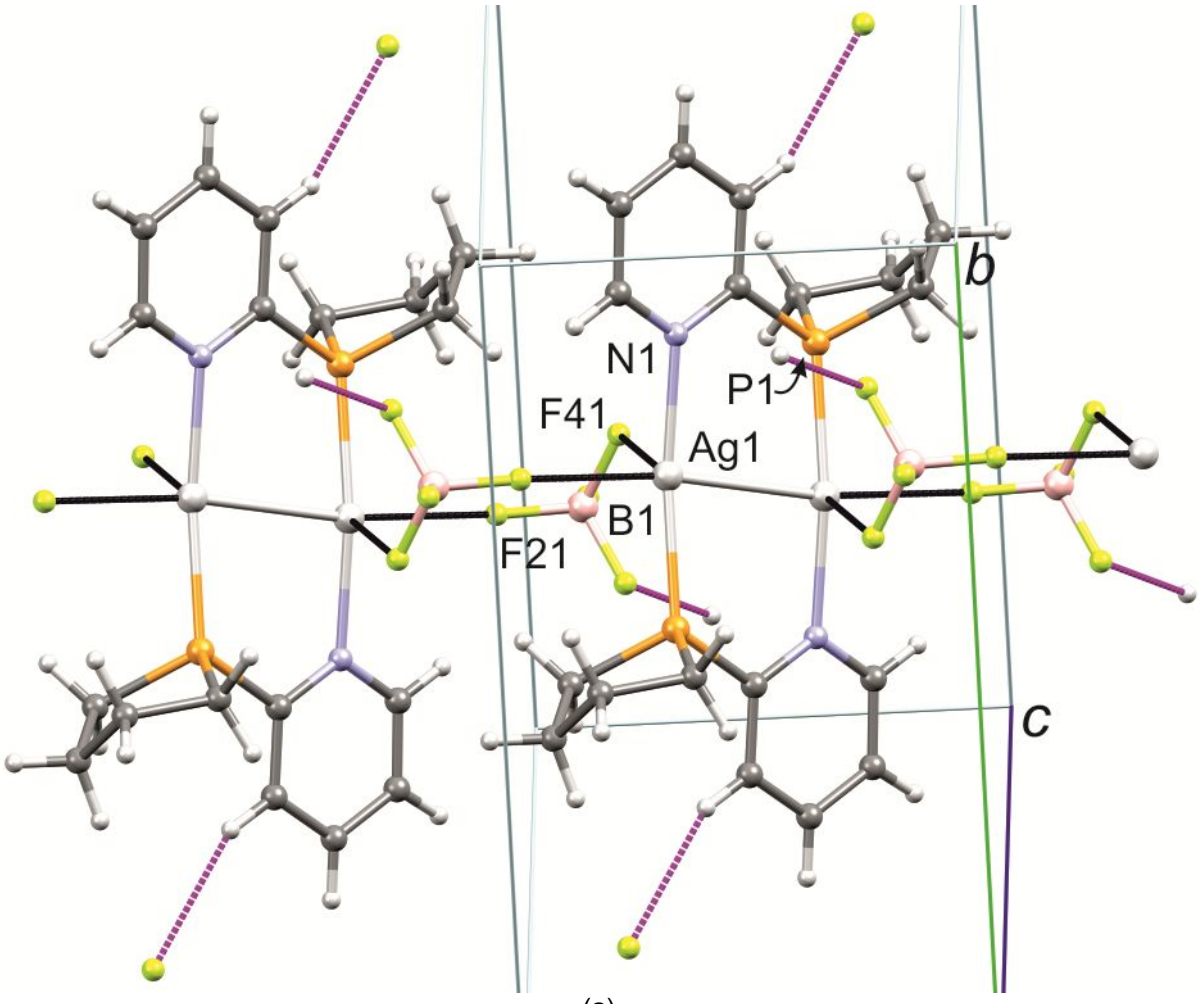

(a)

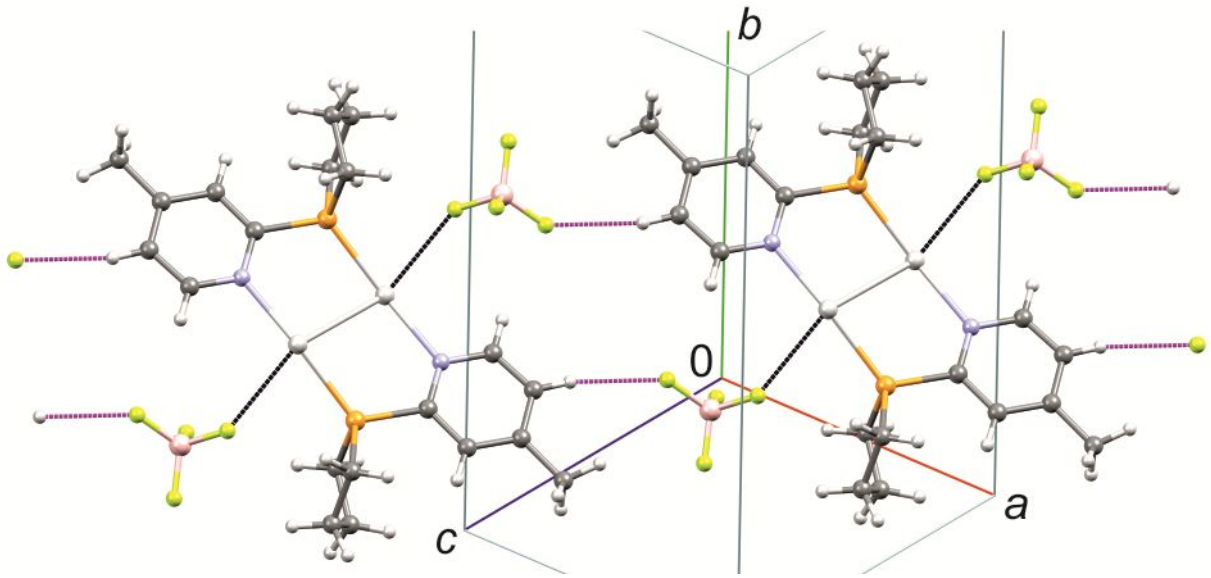

(b)

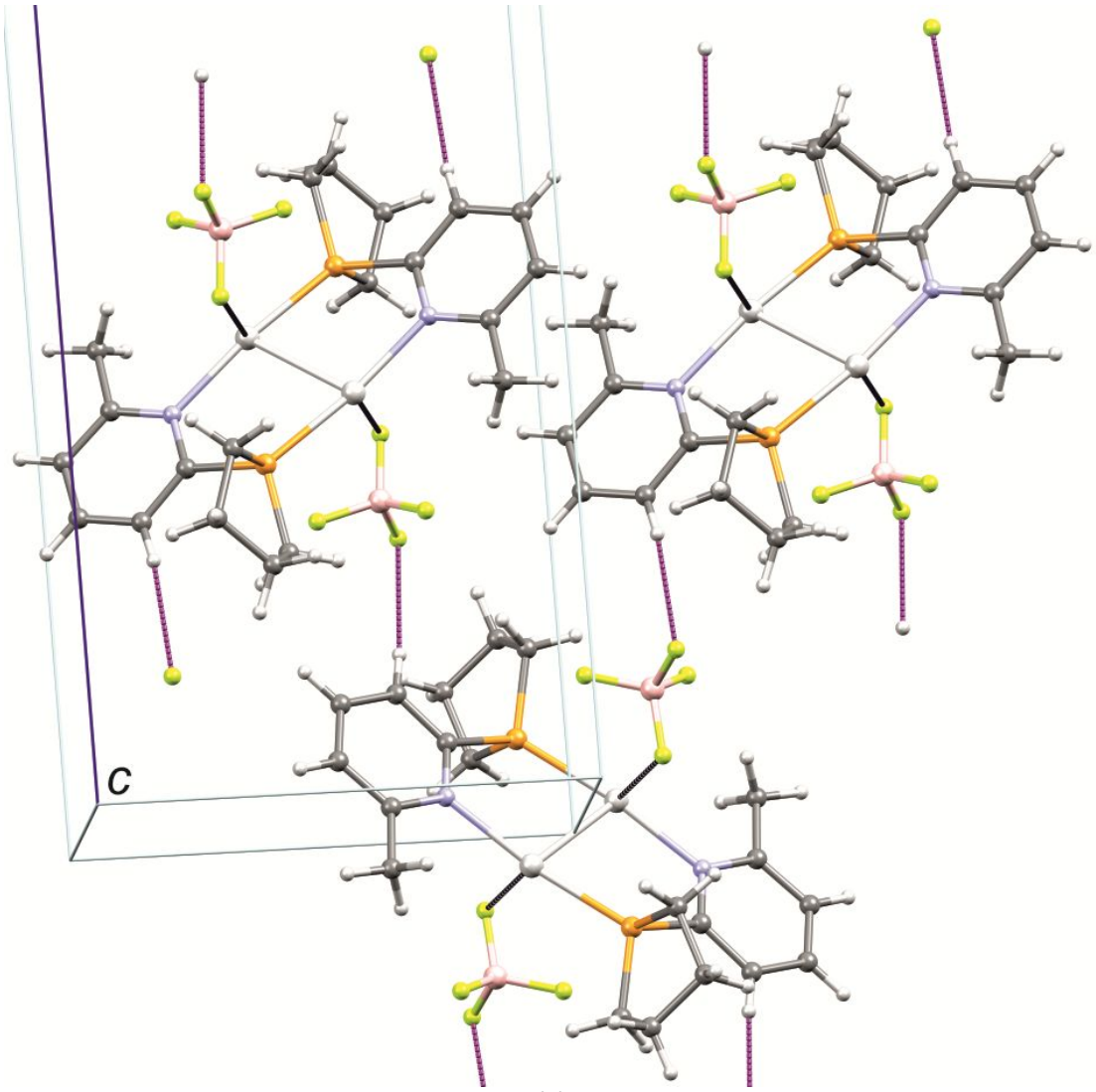

(c)

Figure S14. Fragments of the molecular packing in crystals **4** (a), **5** (b), and **6** (c): Ag···F interactions and C(sp^2)–H···F contacts are marked in black and magenta dotted lines, respectively. In the case of **4** and **5**, only the main component of disordered tetrafluoroborate anions is shown.

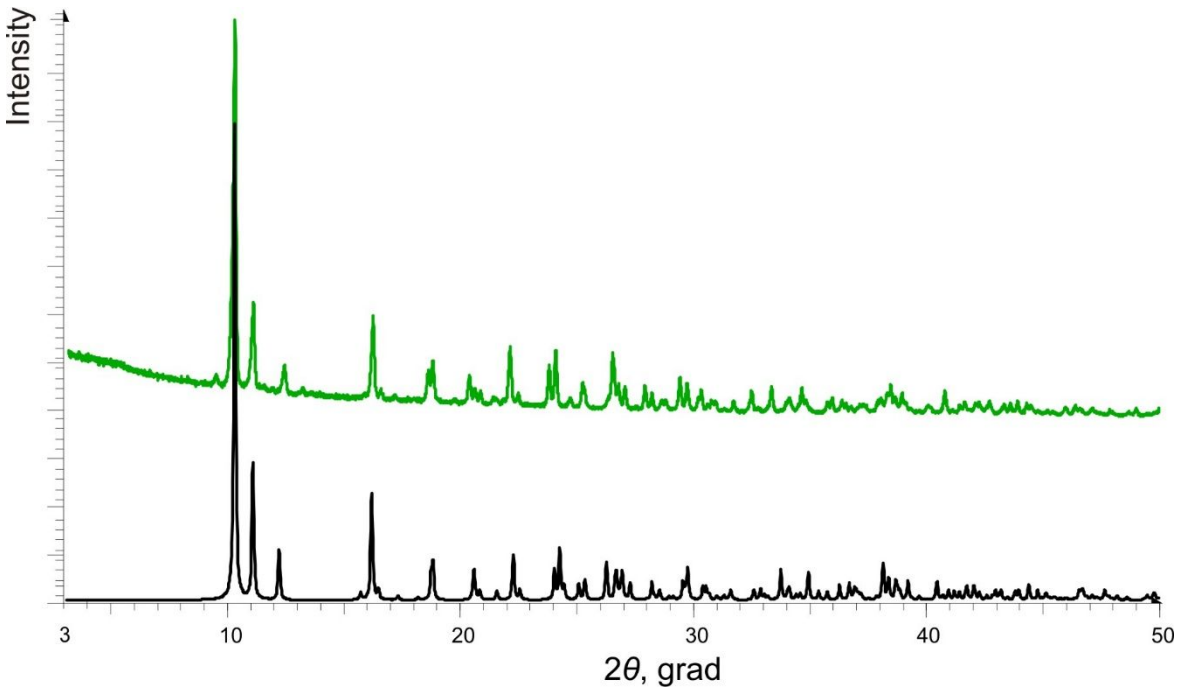

Figure S15. PXRD pattern for complex **4** (green curve is an experimental powder diffractogram (293 K), black one is a theoretical diffractogram calculated from single crystal X-ray data (150K)).

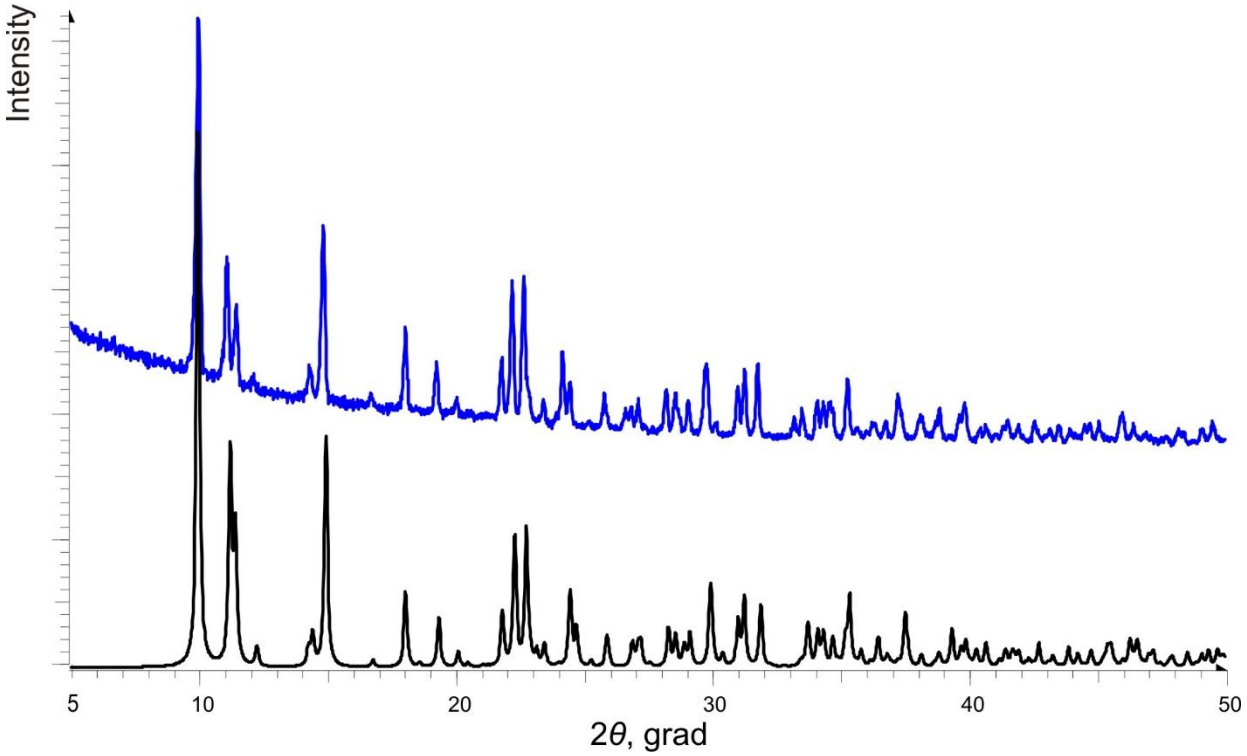

Figure S16. PXRD pattern for complex **5** (blue curve is an experimental powder diffractogram (293 K), black one is a theoretical diffractogram calculated from single X-ray data (173K)).

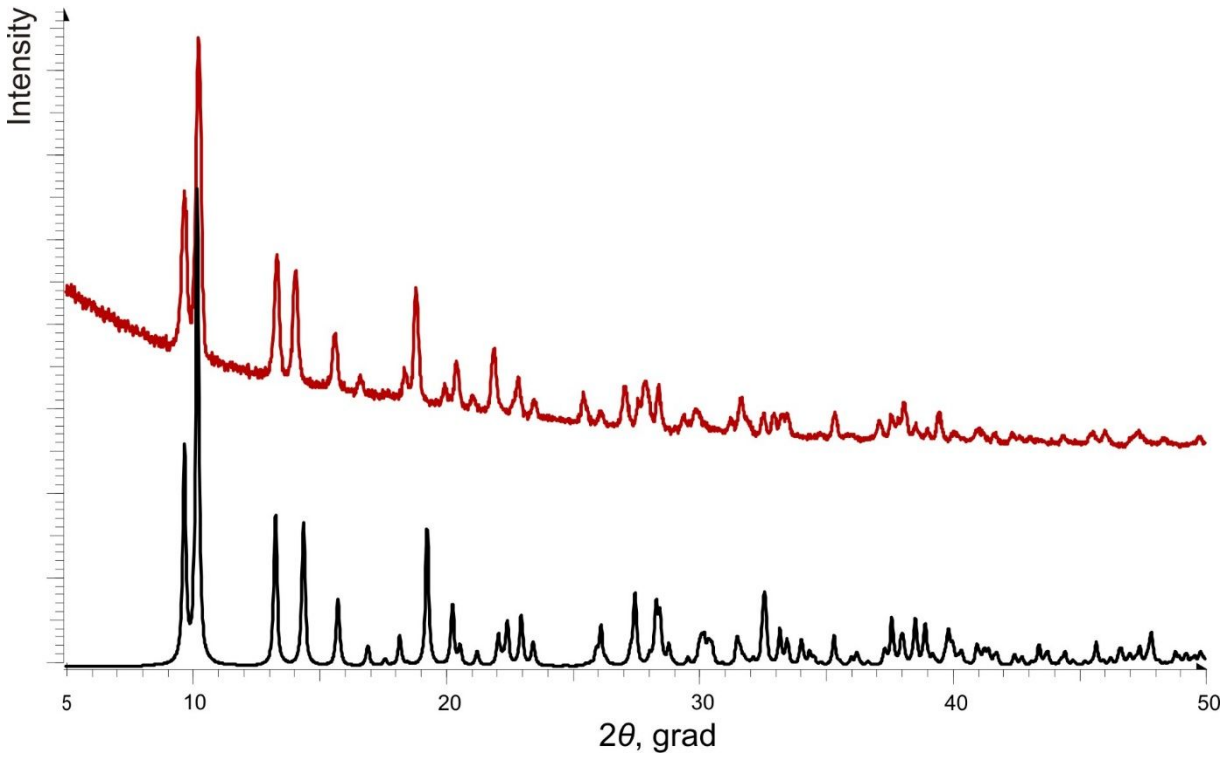

Figure S17. PXRD pattern for complex **6** (red curve is an experimental powder diffractogram (293 K), black one is a theoretical diffractogram calculated from single X-ray data (100K)).

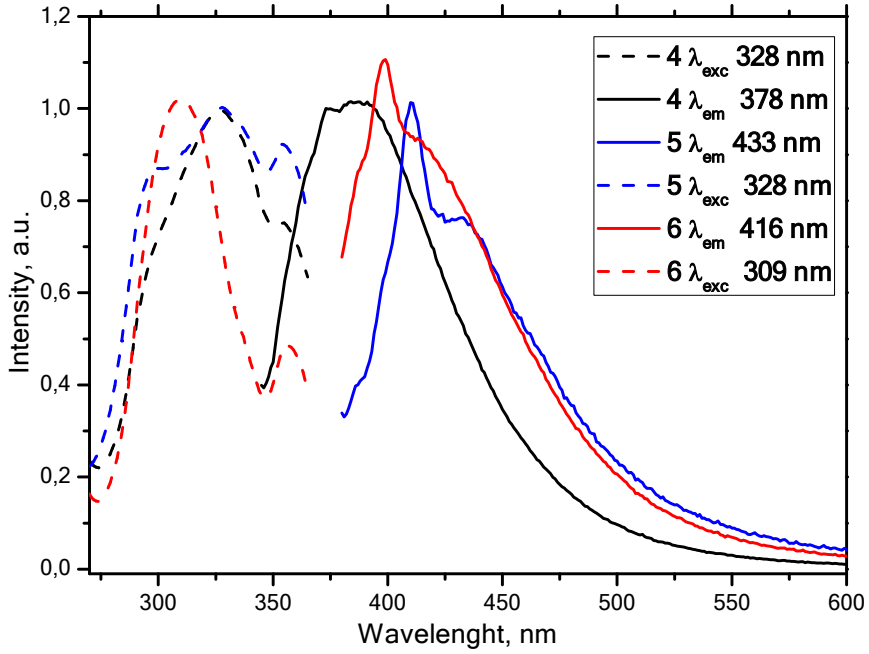

Figure S18. Emission (upon excitation at 335 nm (**4**), 365 (**5**), 355 (**6**)) (solid line) and excitation (for 400 nm) (dashed line) spectra of acetonitrile solutions of **4** – **6** (concentration $2.7*10^{-5}$ mol·L^{-1}).

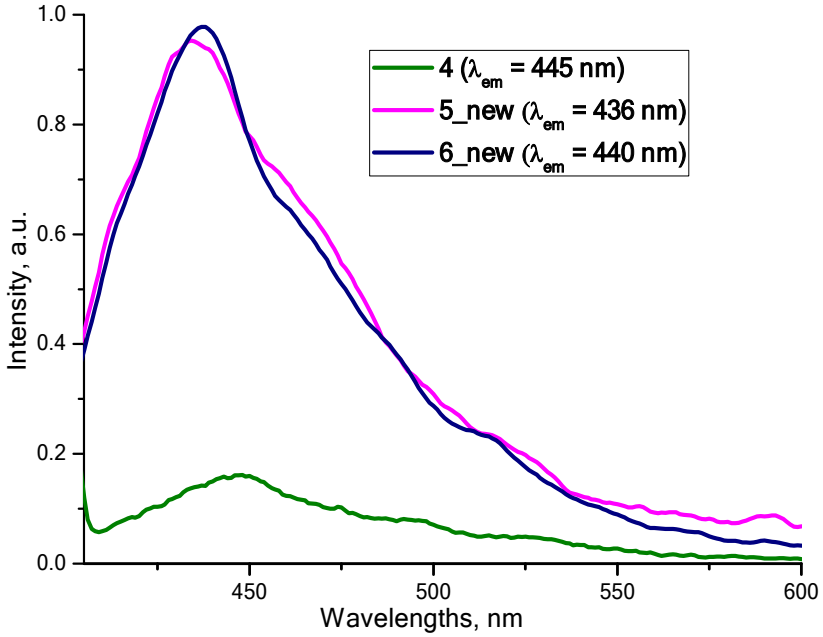

Figure S19. Emission (upon excitation at 340 nm (**4**), 330 (**5**), 373 (**6**)) spectra of **4** – **6** in DMSO solutions (concentration $5*10^{-4}$ mol·L^{-1}).

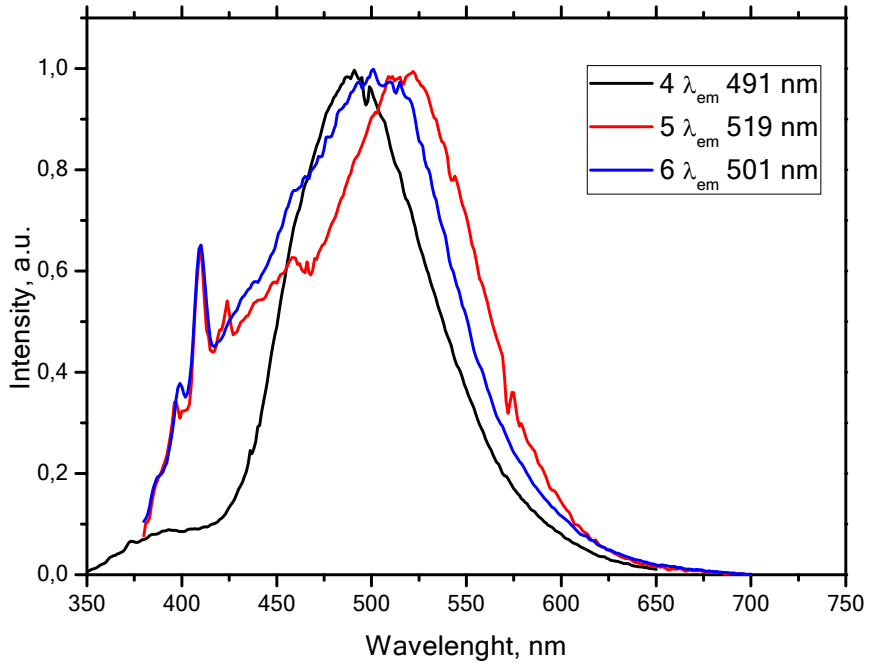

Figure S20. Emission spectra (upon excitation at 335 nm (**4**), 365 (**5**), 355 (**6**)) of complexes **4** – **6** in acetonitrile at 77K (concentration $2.7*10^{-5}$ mol·L^{-1}).

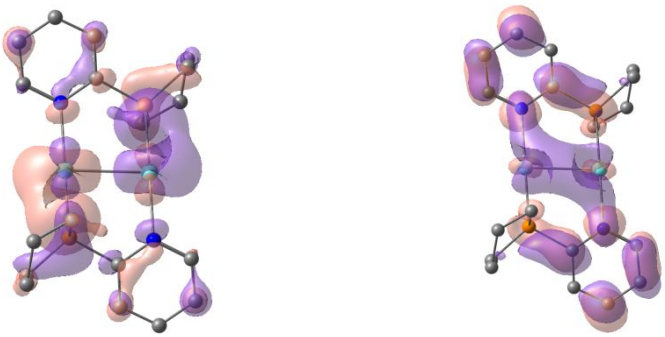

Figure S21. HOMO and LUMO of S_0 state of isolated cationic part of molecule **4** computed on the optimized T_1 state geometry.

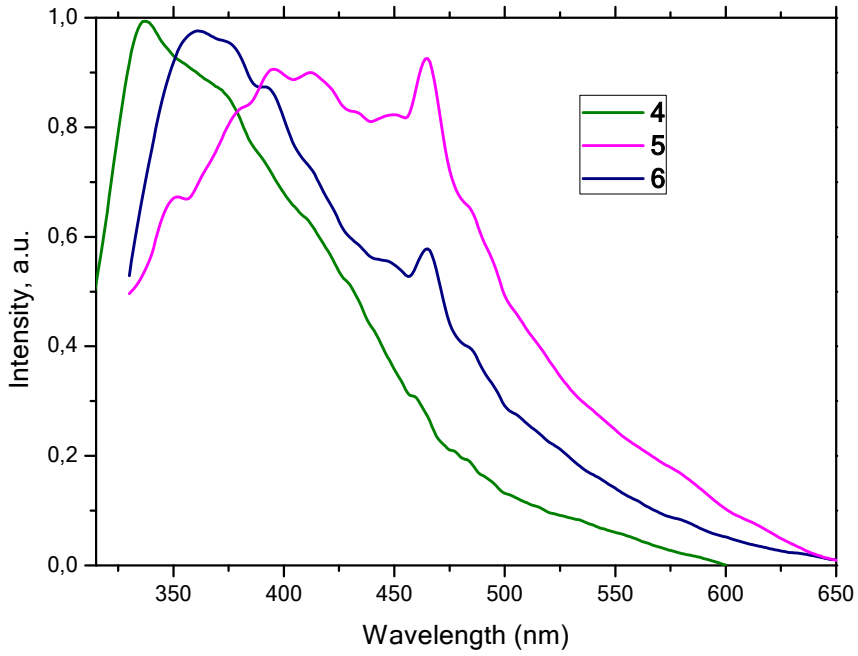

Figure S22. Solid-state excitation spectra of complexes **4** – **6** recorded at 298 K.

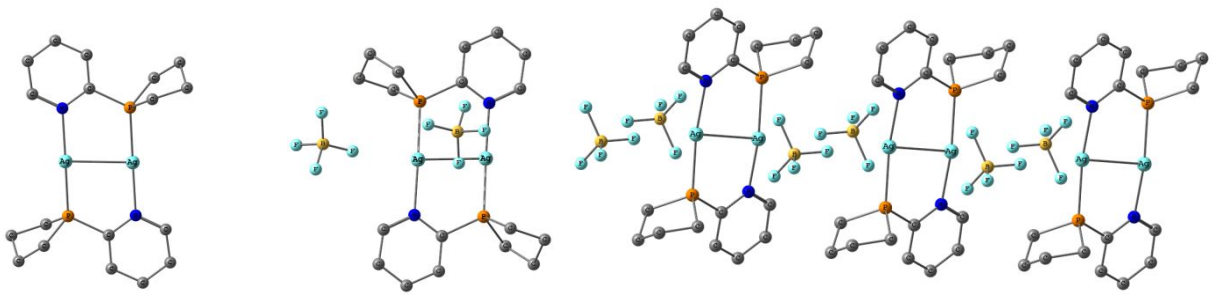

Figure S23. Structures of computationally considered models and the longest wavelengths predicted for their absorption.

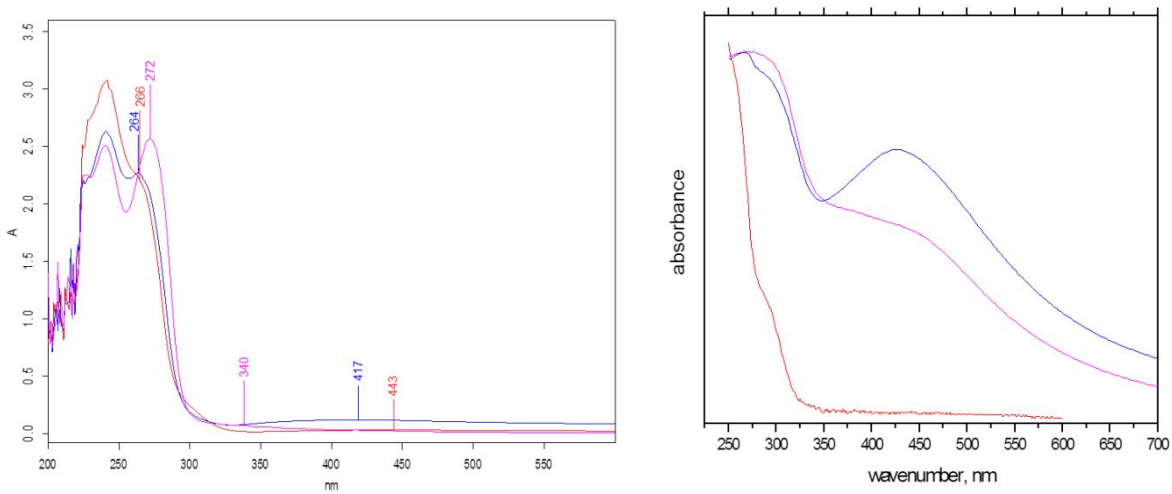

Figure S24. Experimental UV-vis absorption spectra of solid samples of **4** (blue), **5** (red) and **6** (magenta) and of their solutions in acetonitrile ($c=2.7\cdot10^{-5}$ mol·L^{-1}). Extinction coefficients: **4**, 11300 (264 nm) and 550 (417 nm); **5**, 10850 (266 nm) and 150 (443 nm); **6**, 12850 (272 nm) and 300 (340 nm).

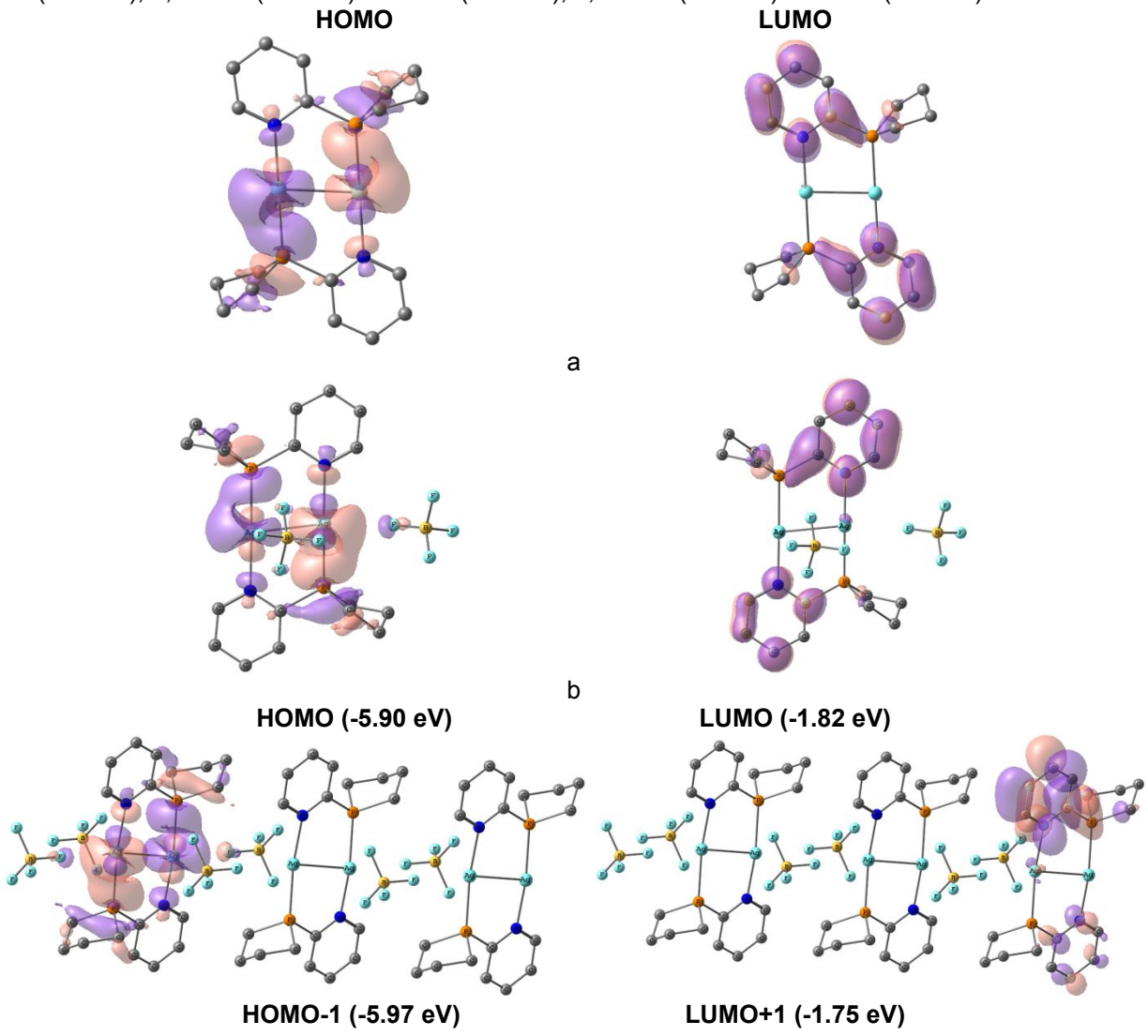

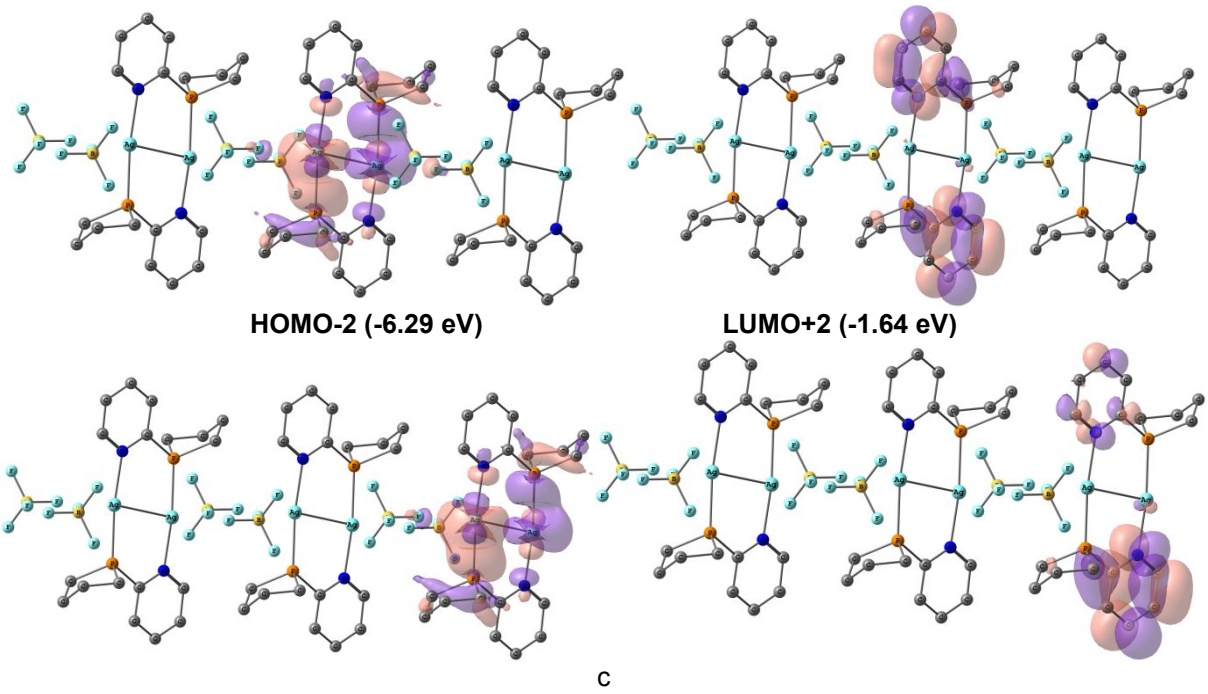

Figure S25. Frontier molecular orbitals of S_0 state of dicationic part of molecule **4** (a), neutral molecule **4** (b) and trimer of molecules **4** (c). In the trimer each of the three molecules **4** has a slightly different environment, which results in a slight splitting of quasi degenerate HOMO and LUMO. Thus, for the trimer model frontier orbitals with close energy values are presented (c).

Table S1. Contribution (in %) of various atoms/fragments into frontier molecular orbitals shown in Figures S21 and S25.

Computed species	HOMO					LUMO				
	Ag	Pyridyl	P	Alk	$[BF_4]$	Ag	Pyridyl	P	Alk	$[BF_4]$
Isolated dication (S_0 state on the optimized T_1 geometry)	43	15	32	9	-	22	67	8	4	-
Isolated dication (S_0 state)	55	7	28	9	-	2	89	5	5	-
Neutral molecule **4** (S_0 state)	53	7	29	9	1	2	90	4	4	0
Trimer of neutral molecules **4** (S_0 state)	53	7	29	9	2	2	90	4	4	0

References

[1] Frisch, M. J.; Trucks, G. W.; Schlegel, H. B.; Scuseria, G. E.; Robb, M. A.; Cheeseman, J. R.; Scalmani, G.; Barone, V.; Petersson, G. A.; Nakatsuji, H.; Li, X.; Caricato, M.; Marenich, A. V.; Bloino, J.; Janesko, B. G.; Gomperts, R.; Mennucci, B.; Hratchian, H. P.; Ortiz, J. V.; Izmaylov, A. F.; Sonnenberg, J. L.; Williams-Young, D.; Ding, F.; Lipparini, F.; Egidi, F.; Goings, J.; Peng, B.; Petrone, A.; Henderson, T.; Ranasinghe, D.; Zakrzewski, V. G.; Gao, J.; Rega, N.; Zheng, G.; Liang, W.; Hada, M.; Ehara, M.; Toyota, K.; Fukuda, R.; Hasegawa, J.; Ishida, M.; Nakajima, T.; Honda, Y.; Kitao, O.; Nakai, H.; Vreven, T.; Throssell, K.; Montgomery, J. A.; Peralta, Jr., J. E.; Ogliaro, F.; Bearpark, M. J.; Heyd, J. J.; Brothers, E. N.; Kudin, K. N.; Staroverov, V. N.; Keith, T. A.; Kobayashi, R.; Normand, J.; Raghavachari, K.; Rendell, A. P.; Burant, J. C.; Iyengar, S. S.; Tomasi, J.; Cossi, M.; Millam, J. M.; Klene, M.; Adamo, C.; Cammi, R.; Ochterski, J. W.; Martin, R. L.; Morokuma, K.; Farkas, O.; Foresman, J. B.; Fox, D. J. Gaussian 16, Revision B.01, Gaussian, Inc., Wallingford CT, 2016.
[2] C. Adamo, V. Barone, *J. Chem. Phys.* **1999**, *110*, 6158–6170.
[3] F. Weigend, R. Ahlrichs, *Phys. Chem. Chem. Phys.* **2005**, *7*, 3297–3305.
[4] S. Grimme, J. Antony, S. Ehrlich, H. Krieg, *J. Chem. Phys.* **2010**, *132*, 154104.
[5] A. D. Becke, E. R. Johnson, *J. Chem. Phys.* **2005**, *123*, 154101.
[6] E. R. Johnson, A. D. Becke, *J. Chem. Phys.* **2006**, *124*, 174104.
[7] S. Grimme, S. Ehrlich, L. Goerigk, *J. Comput. Chem.* **2011**, *32*, 1456–1465.
[8] T. Zhang, C. Ji, K. Wang, D. Fortin, P. D. Harvey, *Inorg. Chem.* **2010**, *49*, 11069–11076.
[9] C. Lee, W. Yang, R. G. Parr, *Phys. Rev. B* **1988**, *37*, 785–789.
[10] A. D. Becke, *J. Chem. Phys.* **1993**, *98*, 5648–5652.
[11] W. J. Hehre, R. Ditchfield, J. A. Pople, *J. Chem. Phys.* **1972**, *56*, 2257–2261.
[12] P. C. Hariharan, J. A. Pople, *Theor. Chim. Acta* **1973**, *28*, 213–222.
[13] W. J. Stevens, H. Basch, M. Krauss, *J. Chem. Phys.* **1984**, *81*, 6026–6033.
[14] W. J. Stevens, M. Krauss, H. Basch, P. G. Jasien, *Can. J. Chem.* **1992**, *70*, 612–630.
[15] T. R. Cundari, W. J. Stevens, *J. Chem. Phys.* **1993**, *98*, 5555–5565.
[16] N. M. O'Boyle, GaussSum 2.0, 2006, available at http:// gausssum.sf.net
[17] G. M. Sheldrick, *Acta Crystallogr. Sect. A: Found. Adv.* **2015**, *71*, 3–8.
[18] G. M. Sheldrick, *Acta Crystallogr. Sect. C: Struct. Chem.,* **2015**, *71*, 3–8.
[19] L. J. Farrugia, *J. Appl. Crystallogr.* **2012**, *45*, 849–854.
[20] A. L. Spek, *Acta Crystallogr. Sect. D Biol. Crystallogr.* **2009**, *65*, 148–155.
[21] E. I. Musina, A. V. Shamsieva, I. D. Strelnik, T. P. Gerasimova, D. B. Krivolapov, I. E. Kolesnikov, E. V. Grachova, S. P. Tunik, C. Bannwarth, S. Grimme, et al., *Dalton Trans.* **2016**, *45*, 2250–2260.